Appl. Phys. A 81, 1303–1307 (2005)
DOI: 10.1007/s00339-004-3051-x

Applied Physics A
Materials Science & Processing

E. TORRES-GARCÍA[1,✉]
A. PELÁIZ BARRANCO[2]
A. HUANOSTA TERA[3]

Analysis of the physical structure of nanometric WO_x/ZrO_2 using electrical measurements

[1] Instituto Mexicano del Petróleo, Eje Central L. Cárdenas 152, México D.F. 07730, Mexico
[2] Facultad de Física, Instituto de Materiales y Reactivos, Universidad de La Habana, San Lázaro y L, Vedado, La Habana 10400, Cuba
[3] Instituto de Investigación en Materiales, UNAM, México D.F. 04510, Mexico

Received: 30 April 2004 / Accepted: 20 September 2004
Published online: 18 November 2004 • **© Springer-Verlag 2004**

ABSTRACT The structure of WO_x/ZrO_2 was studied by X-ray diffraction, laser Raman spectroscopy and measurement of electrical properties using impedance spectroscopy. Results from classical analysis were consistent with a structure comprising nanometric ZrO_2 particles covered by a WO_x surface layer. Based on this information we modelled the impedance spectra as the superposition of two contributions. The values of the electrical properties estimated from our model indicated the presence of a dielectric and a semiconductor. The first phase had electrical properties closely matching the reported values for ZrO_2, whereas the semiconductor phase was assigned to a non-stoichiometric WO_x phase. The tungsten-bearing species had temperature-dependent properties and play an important role in the ac response of the studied system and also in oxidation–reduction processes. The activation energy is 1.3 eV for ZrO_2, whereas WO_x has two slightly different energy values (2.4 and 2.1 eV) in different temperature ranges. Use of impedance spectroscopy provides valuable information about the surface structure as well as the contribution of the bulk, which may be important in catalysis.

PACS 68.35.Bs; 81.05.Ys; 82.65.Dp

1 Introduction

Development of new solid acids has received special attention for years to improve solid materials and because of ecological concerns pointing at the replacement of liquid acids still used as catalysts, particularly in the petrochemical industry. On the other hand, mixed oxides with high acidity have been developed and used as catalysts or supports in reactions such as cracking, isomerization, oxidation, acetylation and others [1–4]. Recently, the WO_x/ZrO_2 system has received much attention because of its good combination of activity and selectivity [3, 5–7]. That is the resultant of balanced surface acid properties, density of acid sites and high thermal stability. In spite of the different studies made, the structure of the active surface species has not been fully understood. A major complication is the fact that catalysis occurs at the surface of the solids, and it is difficult to probe it.

✉ Fax: +52-55-91758429, E-mail: etorresg@imp.mx

The structure of the active material is peculiar, inasmuch as a metastable structure has to be attained [2, 3, 7, 8]. It is generally agreed that catalytically active WO_x/ZrO_2 consists of nanometric particles of tetragonal zirconia stabilized by a surface layer of WO_x, where $x > 3$.

The analysis of the structure of solid catalysts has relied heavily upon spectroscopic techniques, such as infrared, Raman, X-ray photoelectron spectroscopy (XPS), X-ray absorption spectroscopy (XAS), high resolution electron microscopy (HREM) and others. The catalysts generally consist of a mixture of ceramics and metals, i.e. insulators and conductors. Some researches have been developed to determinate their electrical properties as a function of temperature and significant efforts have been made in establishing structure–property relationships, which are very important for practical applications.

To investigate electrical features of WO_x/ZrO_2, we decided to study it by using impedance spectroscopy [10], a powerful technique for determining electrical properties of materials. It is interesting for our purposes because the experimentally observed frequency dependence of the impedance contains information about intragranular and interfacial regions in the material being studied, as well as about their interrelations. The information can be extracted by modelling the spectra using simple equivalent electrical circuits, each of them corresponding to different structural units of the material. Some characteristics of the circuits may be suggested by direct observation of the resultant impedance plots, coupled with structural information gathered with other techniques. Impedance spectroscopy allows us to determine not only the electrical properties, but also the structure of the phases composing WO_x/ZrO_2. We are analysing the extension of this methodology to other so-called monolayer systems, a group of industrially important catalysts.

2 Experimental procedure

We prepared a WO_x/ZrO_2 sample by selective precipitation from aqueous solution [9, 14, 15] The $(NH_4)_6H_2W_{12}O_{40}$ (Strem Chemicals, 99.9%) and $ZrOCl_2$ (Aldrich, > 98 wt. %, Hf 0.5 wt. %) solutions (0.5 M each) were mixed and then hydrolysed under stirring by addition of a NH_4OH (Baker 28%) solution until the pH was 10. The precipitate was filtered and then washed repeatedly by redis-

persion in a NH_4OH solution (pH = 10) until the chlorine level was below 10 ppm. We dried the filtrate at 383 K during 15 h, and then heated the resulting solid at 5 K/min to 1073 K and kept it for 3 h at this temperature. The chemical analysis, after calcinations at 1073 K, was carried out using a plasma optical emission spectrometer (Perkin Elmer model 400). This method of synthesis resulted in samples containing about 10 wt. % tungsten.

The sample was characterized by using X-ray diffraction (XRD, model D500, Siemens) with Cu K_α radiation at a scanning rate of $0.003^\circ\ s^{-1}$. The Scherrer relationship was used to calculate the crystallite size of zirconia using the (1 1 −1) and (1 1 1) reflections of the monoclinic and tetragonal phases. Quartz was used for instrumental calibration.

The Raman spectra of the WO_x/ZrO_2 sample were obtained with an Ar^+-ion laser (Ionics, model 1400-5A) delivering about 30–40 mW of incident radiation. The excitation line of the laser was 514.5 nm. The Raman spectrometer was a double-monochromator device (SPX, model 1403). Measurements were made at room temperature.

The ac response of WO_x/ZrO_2 was measured by using an impedance analyser (model 4192A, Hewlett-Packard) controlled by a microcomputer. The frequency range scanned was 5 Hz to 13 MHz, using 1 V as the applied voltage in all cases. The measurements were made isothermally in air between 296 and 1103 K. Although electrical measurements of ceramic materials are commonly performed on sintered samples, in our case high-temperature sintering would cause phase separation ($WO_x/ZrO_2 \rightarrow WO_3 + ZrO_2$) and loss of the structure responsible for catalysis. In view of that, we prepared samples by cold pressing powders and placing gold electrodes on opposite faces of the coin-shaped pellets.

3 Results and discussion

3.1 *Structure*

Below 1073 K, the diffraction pattern of WO_x/ZrO_2 indicated that the tetragonal phase of ZrO_2 was dominant (Fig. 1). Rietveld refinement of the diffraction pattern of WO_x/ZrO_2 gave the following unit-cell parameters: $a = 3.5994(10)$ Å, $c = 5.1507(13)$ Å and $V = 66.73$ Å [9, 13]. These values were very close to those reported for the metastable tetragonal phase of pure ZrO_2 [12, 13]. The agreement between the unit-cell parameters for ZrO_2 in WO_x/ZrO_2 and those of pure tetragonal ZrO_2 is a clear indication of the absence of a solid solution. Furthermore, the estimated average ZrO_2 grain size for metastable WO_x/ZrO_2 was about 20 nm [1, 14, 15]. The surface presence of WO_x species stabilized the tetragonal crystalline structure of the ZrO_2 nanometric particles presumably by restricting oxolation and intercrystallite sintering. Also, the lack of reflections in the X-ray patterns related with specific tungsten oxo-species in the samples suggested that WO_x species were highly dispersed on the surface of the ZrO_2 nanoparticles.

Figure 2 shows the Raman spectra of WO_3, ZrO_2 and WO_x/ZrO_2 samples containing about 10 wt. % of tungsten. The ZrO_2 tetragonal phase can be identified from the peak at 647 cm^{-1}, while the presence of the Raman bands of about 617 and 637 cm^{-1} are associated with the ZrO_2 monoclinic phase [2, 9, 11, 16–20]. The signals corresponding

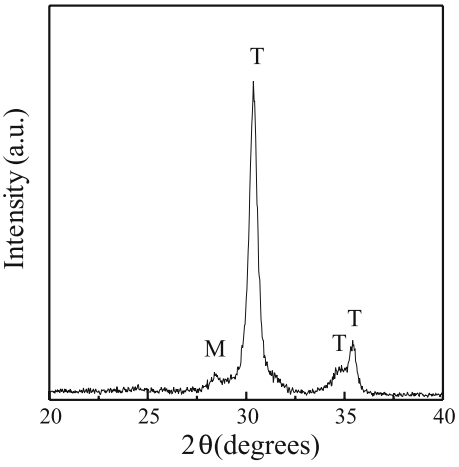

FIGURE 1 X-ray diffraction pattern of 9.7 wt. % W in WO_x/ZrO_2 calcined at 1073 K as an example of the characteristic behaviour for samples containing about 10 wt. % tungsten. T and M indicate the tetragonal and monoclinic zirconia phases, respectively

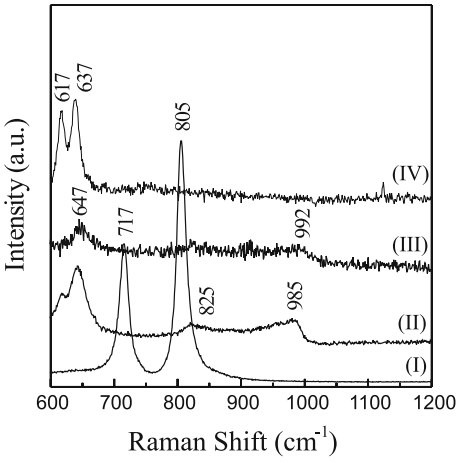

FIGURE 2 Raman spectra of WO_x/ZrO_2 samples calcined at 1073 K. Characteristic profile of the samples containing about 10 wt. % tungsten are shown: (I) polycrystalline WO_3, (II) 10.5 wt. % W, (III) 9.7 wt. % W and (IV) crystalline ZrO_2 calcined at 773 K

to reported surface tungsten oxo-species were expected in the 700–1060 cm^{-1} region for W−O−W modes and W=O stretching modes [17–20]. We observed a shoulder at about 985–992 cm^{-1}, which is assigned to the symmetric stretch mode of terminal W=O bonds, attributed to tungsten species showing various degrees of polymerization [8, 18]. We did not detect the strong bands at 715 and 807 cm^{-1}, which are characteristic of WO_3, even when the samples were heated above 1073 K, i.e. even when the WO_x metastable tetragonal ZrO_2 composite was destroyed.

From our previous results, as well as the experimental evidence obtained in this study, we can conclude that the obtained WO_x/ZrO_2 consists primarily of a matrix of nanometric tetragonal ZrO_2 covered with tungsten oxo-species, in agreement with previous reports [1–3, 9, 14, 15].

3.2 *Electrical measurements*

In single-phase systems, the complex impedance plane (Z'' vs. Z', where Z' and Z'' are, respectively, the

real and imaginary components of the impedance) consists of a regular semicircle. It is modelled as a resistance–capacitance (RC) parallel circuit [21]. The resistance (R) is usually determined from the low-frequency intercept of the semicircle on the real axis (Z'), whereas the capacitance (C) is estimated from the maximum of the semicircle. At that point, $\omega_{max} RC = 1$, where $\omega_{max} = 2\pi f_{max}$ (f_{max} is the frequency at the maximum of the semicircle).

Polycrystalline materials show complex responses resulting from the overlap of the signals from the different components. In such cases, circuit simulations are needed in order to separate each contribution. Frequently structural information is used in order to determine the equivalent circuit that best meets all the requirements. Once that is done, the RC parameters are calculated as in a single-phase material.

The impedance spectra for our sample were obtained at several temperatures. Below 573 K there was only an ill-defined arc in the impedance plane. As the temperature increased, conduction increased and the global signal had two branches, as can be seen in Fig. 3, where two temperatures are presented as examples of the general behaviour. The small branch at the low-frequency range of the impedance plots corresponds to electrode effects and was not analysed further. As we were using ion-blocking electrodes, the presence of a spike at the low-frequency branch would reveal the presence of ionic species, if they were moving. The absence of a spike at the tail of the small arc indicated that conduction in our material was primarily electronic [21].

The high-frequency signal in the impedance plane for WO_x/ZrO_2 was a deformed semicircle, indicating that the electrical response of this material was composed of two or more overlapping individual signals. We analysed various element arrangements that could describe the electrical response of the samples [10]. From analysis of previous reports for this system [2, 9] and our XRD and Raman results presented previously in this work, we concluded that the physically correct equivalent circuit consisted of two RC parallel

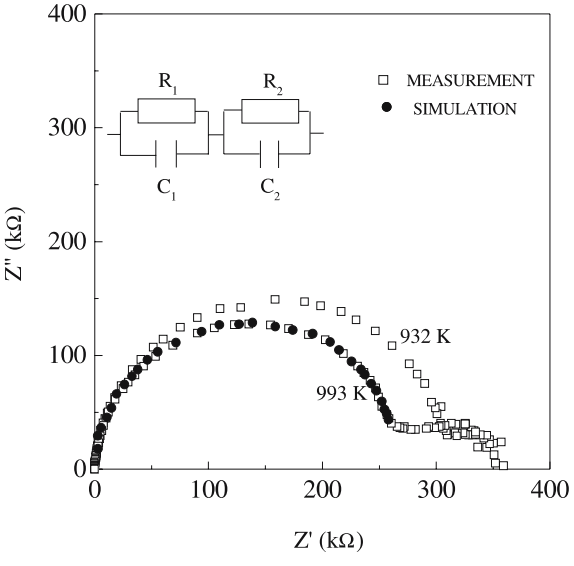

FIGURE 3 Characteristic behaviour of the complex impedance planes as a function of the temperature for the WO_x/ZrO_2 system. Two temperatures are shown as examples of the general behaviour

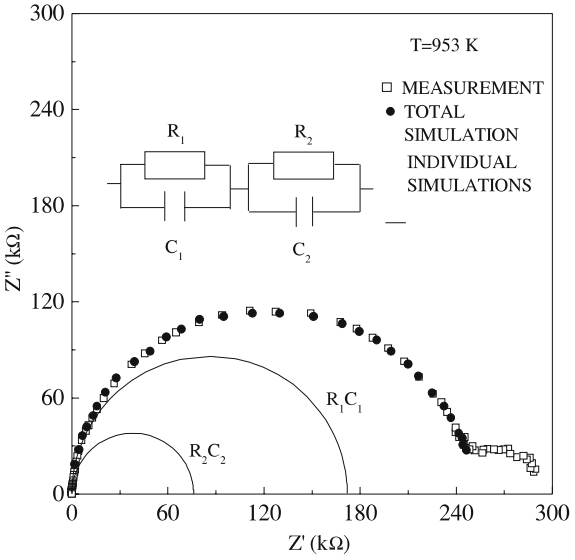

FIGURE 4 Complex impedance planes for WO_x/ZrO_2 at 953 K, as an example of the characteristic behaviour. The deconvolution corresponding to the overlapping semicircles representing each phase is shown, as well as the equivalent circuit

arms connected in series, shown in Fig. 4 for 953 K, as example of the characteristic behaviour for samples containing about 10 wt. % tungsten. Equation (1) describes the complex impedance (Z) of the material, where the subscripts 1 and 2 correspond to each of the phase contributions. The equation has been obtained considering the equivalent circuit; the R and C values corresponding to each of the overlapping semicircles were determined by non-linear least-squares [22] for each temperature. The overall fit was excellent at each of the analysed temperatures.

$$Z(\omega) = \frac{R_1}{1+(\omega R_1 C_1)^2} + \frac{R_2}{1+(\omega R_2 C_2)^2} - \mathrm{j}\left[\frac{\omega C_1 R_1^2}{1+(\omega C_1 R_1)^2} + \frac{\omega C_2 R_2^2}{1+(\omega C_2 R_2)^2}\right]. \quad (1)$$

3.3 *Relationship between structure and electrical response of each phase*

As mentioned before, our selection of the final equivalent circuit was based on the need to be consistent with the presence of a bulk ZrO_2 phase and a WO_x surface phase in WO_x/ZrO_2, determined by X-ray diffraction, Raman spectroscopy as well as HREM and its numerical simulations of the model particles and other techniques [2, 9, 14, 15]. Once that was set, we analysed for self-consistency among the calculated values of C and the proposed phases. The magnitude of the capacitance and its temperature dependence provide criteria for establishing the relationship between each semicircle, i.e. each phase, and the pertinent microstructural features of the material [23].

The high-frequency contribution (R_1, C_1) exhibited C-values of the order of 10^{-11} F, usually associated with the bulk response of grains [23]. The capacitance remained almost constant with temperature (Fig. 5, full symbols), a characteristic behaviour of classical dielectrics. The resistivity at

813 K was $10^5\ \Omega$ cm. There are reports about the resistivity of ZrO_2 changing from 10^6 to $10^4\ \Omega$ cm in the 650–970-K range [24, 25]. We also estimated the activation energy for the intrinsic conductivity of the high-frequency component from the slope of the Arrhenius curve (Fig. 6, full symbols). The obtained value ($E_a = 1.32$ eV) is close to the reported activation energy for the intrinsic conductivity in ZrO_2, 1.12 eV [24]. Based on the electrical information and the structural characterization described previously, we assigned the high-frequency component to the ZrO_2 nanocrystals. Another detail worth mentioning is that the activation energy for conduction in the dielectric phase was approximately constant in the studied temperature range, i.e. the structure did not change. We have determined that ZrO_2 remains tetragonal below 1073 K in WO_x/ZrO_2 when this material is prepared according to the method described in this article and elsewhere [2, 3, 8, 16, 18]. Thus, the last experimental point, at high temperatures in the Arrhenius curve, may indicate that the tetragonal phase has gone.

Capacitance values of the order of 10^{-10} F were obtained from the low-frequency component (Fig. 5, open symbols). Although those values are generally associated with grain boundaries, this is true when ions are the main current-carrying species [23]. Our assignment differs for a number of reasons. First, large charges are not flowing through the sample. Second, there are reports of capacitance values similar to those obtained in this study being exhibited by a second phase [23]. Finally, as we were dealing with a pressed powder rather than with a sintered sample, there must be expected an electrical response as a combination of two well-defined components. So, it has been concluded that the second semicircle corresponds to the electrical properties of a second component, namely WO_x surface species.

In the studied temperature range, the capacitance values assigned to WO_x species show a temperature dependence, exhibiting two dispersive stages around 923 and 1035 K (Fig. 5). Two characteristics are pointed out here. Regarding the dispersive stage around 925 K, it should be linked with the behaviour exhibited by the corresponding Arrhenius curve, particularly the sudden decrease in conductivity slightly below 950 K, open symbols in Fig. 6, which shows the typical shape of a non-degenerate extrinsic semiconductor [26]. On the other hand, the behaviour observed around 1035 K may originate from partial reduction of WO_x regions, an aspect that has been recently discussed [27]. It is worth noting that heating WO_x/ZrO_2 causes the formation of dark-coloured partially reduced oxides. A surface-reduction process could provide electrons and change this material into an *n*-type donor semiconductor, enriching the total conductivity. This would establish a link between dielectric relaxation and electrical conduction. This means that the dielectric dispersion observed at 923 and 1035 K, open symbols in Fig. 5, must be related to the mechanism of charge conduction, which should be electronic charge carriers jumping between permitted sites. It also promotes a considerable dipolar activity in the WO_x species at the mentioned temperatures. The activation-energy values of the two components in WO_x/ZrO_2 are given in Table 1. Also, it is very important to note that although the system is of nanometric order, its electrical behaviour is of one typical bulk, in both of the phases present.

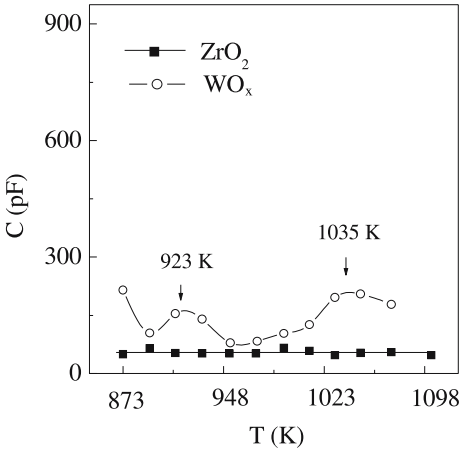

FIGURE 5 Temperature dependence of the capacitance of each phase in WO_x/ZrO_2. The high-frequency contribution (*full symbols*) is associated with the ZrO_2 nanocrystals and the low-frequency contribution (*open symbols*) is associated with the WO_x surface species

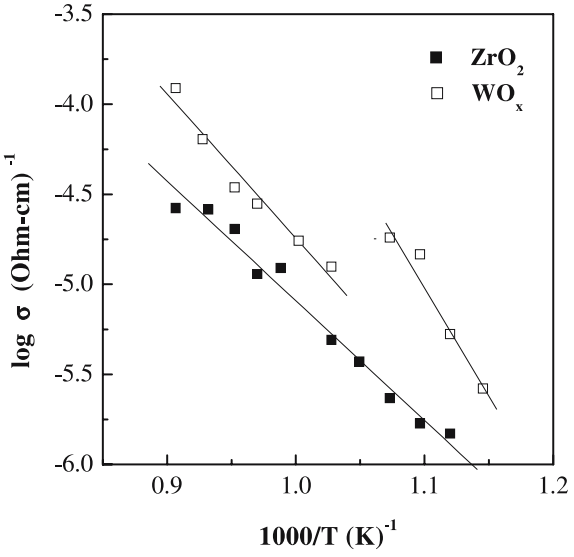

FIGURE 6 Arrhenius dependence of the conductivity for each phase in WO_x/ZrO_2

Based on the electrical measurements, the results suggest a direct relation between the electrical conductivity and the density of defects, originating by partial reduction of W atoms on the surface. Then, atoms in the vortex structures during the heating can generate unsatisfied coordination sites with high surface energy, providing the increase of the total electrical conductivity. These coordinately unsaturated W^{6+} ions would act as Lewis-acid sites. The acidity of these sites might be very strong, according to the high charge, the quite small ionic radii (0.58 Å for octahedrally coordinated W atoms) and the high electronegativity ($x_i = 22.1$ of the cation) [28].

This study indicates that the analysis of the ac response of systems forming monolayer structures is useful to determine their structure and the properties of the bulk and surface phases. This also shows that the interaction of a nanostructured material with an applied ac field can render important physical information and that, although the system is of nano-

Temperature range (K)	E_a (ZrO_2) (eV)	E_a (WO_x) (eV)
$873 \leq T \leq 1035$	1.32 ± 0.03	2.44 ± 0.03
$1035 < T \leq 1103$	1.32 ± 0.03	2.16 ± 0.03

TABLE 1 Activation-energy values for conduction in granular (ZrO_2) and surface (WO_x) phases of WO_x/ZrO_2

metric order, its electrical behaviour is of typical bulk. As in the present case, the electrical characterization of the WO_x surface species and its relationship with the electronic conductivity could be useful in order to evaluate possible practical systems, essentially for oxidative desulphurization reactions [2]. The thermal activation process generates surface defects; this means that there must be a large quantity of hot points per unit area that is directly related to the chemical potential and catalytic activity, promoting an increase of the charge-carrier density.

4 Conclusions

It is remarkable that we have used the ac technique to determine structural characteristics of different temperature-dependent conducting phases of an un-sintered solid system. As discussed, it was done in particular for WO_x/ZrO_2, which is an important catalytic system. The electrical response of WO_x/ZrO_2 obtained by impedance spectroscopy was modelled as a combination of two phases, whose main electrical features were simulated by two parallel RC elements in series. Using impedance data we determined the temperature dependence of conductivity of each phase.

The results indicate a direct relation between the electrical conductivity and the density of defects, originating by partial reduction of W^{6+} atoms on the surface.

Analysing the worked out parameters and comparing them with those in the literature, we conclude that our results are consistent with a physical structure consisting of nanometric ZrO_2 crystallites covered by surface WO_x species. So, in our opinion this work opens up the possibility to carry out systematic investigations about structural properties of catalytic systems through ac measurements.

ACKNOWLEDGEMENTS The authors thank Dr. F. Calderón and Dr. E. Haro-Poniatowski for useful discussions. Special thanks go to the ICTP, Trieste, Italy for financial support of the Latin-American Network of Ferroelectric Materials (NET-43).

REFERENCES

1 E. Iglesia, D.G. Barton, S.L. Soled, S. Miseo, J.E. Baumgartner, W.E. Gates, G.A. Fuentes, G. Meitzner: Stud. Surf. Sci. Catal. **101**, 533 (1996)
2 E. Torres-García, G. Canizal, S. Velumani, L.F. Ramírez Verzdusco, F. Murrieta-Guevara, J.A. Ascencio: Appl. Phys. A **79**, 2037 (2004)
3 L.F. Ramírez-Verduzco, E. Torres-García, R. Gómez-Quintana, V. González-Peña, F. Murrieta-Guevara: Catal. Today (2004), DOI: 10.1016/j.cattod.2004.07.042
4 M. Hino, K. Arata: J. Chem. Soc. Chem. Commun. 1259 (1987)
5 C.D. Baertsch, K.T. Komala, Y.H. Chua, E. Iglesia: J. Catal. **205**, 44 (2002)
6 R.D. Wilson, D.G. Barton, C.D. Baertsch, E. Iglesia: J. Catal. **194**, 175 (2000)
7 S. De Rossi, G. Ferraris, M. Valigi, D. Gazzoli: Appl. Catal. A **231**, 173 (2002)
8 M. Valigi, D. Gazzoli, I. Pettiti, G. Mattei, S. Colonna, S. De Rossi, G. Ferraris: Appl. Catal. A **231**, 159 (2002)
9 E. Torres-García, G. Rosas, J.A. Ascencio, E. Haro-Poniatowsky, R. Pérez: Appl. Phys. A **79**, 401 (2004)
10 J. Ross Macdonald (Ed.): *Impedance Spectroscopy* (Wiley, New York 1987)
11 P.D.L. Mercera, J.G. Van Ommen, E.B.M. Doesburg, A.J. Burggraaf, J.R.H. Ross: Appl. Catal. **57**, 127 (1990)
12 J. Málek, L. Benes, T. Mitsuhahi: Powder Diffr. **12**, 96 (1997)
13 L.C. Hammond, J.L. Cocking: Powder Diffr. **11**, 75 (1996)
14 E. Torres-García: 'Preparación y Caracterización de Oxoespecies de Wolframio Dispersas Sobre Oxido de Circonio WO_x/ZrO_2'. PhD Thesis, Havana University, Cuba, 2000
15 E. Torres, A. Peláiz, F. Calderón, G.A. Fuentes: Proceeding of IX Latin-American Congress on Surface Science and Applications (July 5^{th}–9^{th}, La Habana, Cuba), *Surface Science and its Applications*, ed. by O. Melo, I. Hernández (World Scientific, 2000) pp. 17–19
16 J. Engweirler, J. Harf, A. Baiker: J. Catal. **159**, 259 (1996)
17 D.S. Kim, M. Ostromecki, I.E. Wachs, S.D. Kohler, J.G. Ekerdt: Catal. Lett. **33**, 209 (1995)
18 S.R. Vaudagna, S.A. Canavese, R.A. Comelli, N.S. Figoli: Appl. Catal. A **168**, 93 (1998)
19 C. Urlacher, J. Mugnier: J. Raman Spectrosc. **27**, 785 (1996)
20 B. Zhao, X. Xu, J. Gao, Q. Fu, Y. Tang: J. Raman Spectrosc. **27**, 549 (1996)
21 A. Peláiz Barranco: 'Propiedades Ferroeléctricas y Mecanismos de Conductividad en el Sistema PZT Modificado'. PhD Thesis, Havana University, Cuba, 2001
22 B.A. Boukamp: *Equivalent Circuit Estimator* (equiver.pas). University of Twente, Department of Chemical Technology, The Netherlands, 1989
23 J. Irvine, D. Sinclair, A. Wets: Adv. Mater. **2**, 132 (1990)
24 http://www.wwwebpro.com
25 http://www.physics.technion.ac.il
26 P.V. Pavlov, A.F. Jojlov: *Física del Estado Sólido* (Mir, Moscow 1987)
27 S. Kuba, P. Concepción Heydorn, R.K. Grasselli, B.C. Gates, M. Che, H. Knözinger: Phys. Chem. Chem. Phys. **3**, 146 (2001)
28 G. Ramis, C. Cinzia, A.S. Elmi, P. Villa, G. Busca: J. Mol. Catal. **61**, 319 (1990)